# Low-frequency wind noise correlation in microphone arrays[a)]

F. Douglas Shields[b)]
*Miltec Research and Technology, Coliseum Drive, University, Mississippi 38677*

(Received 2 July 2004; revised 2 February 2005; accepted 2 February 2005)

A three-axis orthogonal microphone array with ten sensors in each arm has been used to study wind noise in the frequency range from 0.05 to 50 Hz. Simultaneous measurements were made of the three components of the varying wind velocity. Measurements have been made for wind speeds from 4 to 7 m/s at three different sites. The frequency-dependent correlation of the wind noise over a range of wind velocities and atmospheric and environmental conditions in the downwind direction varies as $\exp(-3.2X)\cos(2\pi X)$. For the crosswind and vertical directions, the correlation decays approximately as $\exp(-7Y)$, where $X$ is the separation in wavelengths in the downwind direction and $Y$ is this separation in the crosswind or vertical direction. Over a limited range of wave numbers, the power density spectra of the varying wind velocity varied as the wave number to the $-\frac{5}{3}$ power and the pressure spectra as the $-\frac{7}{3}$ power. © *2005 Acoustical Society of America.*
[DOI: 10.1121/1.1879252]

PACS numbers: 43.28.Ra, 43.28.Dm, 43.28.-g [DKW] Pages: 3489–3496

## I. INTRODUCTION

Current efforts to monitor low-level nuclear explosions in the atmosphere and to detect battle-field infrasound have increased interest in separating infrasound from wind noise in outdoor microphone signals. This wind noise increases dramatically with decreasing frequency. For more than 50 years pipe arrays have been employed to average pressure variations over an extended surface area and thus separate infrasound from wind noise.[1–3] Because sound travels approximately 100 times faster than wind, pressure ports in the pipe arrays can be separated far enough to get random signals from the wind and still get coherent signals from sound. If the pressure variations due to the wind are incoherent, the averaging process will reduce the pressure spectrum by a factor of $1/n^{1/2}$ or the power density spectrum by a factor of $1/n$, where $n$ is the number of ports. To design such arrays it is necessary to know how the correlation of the wind-induced pressure variations depends on the sensor separation.

This paper reports wind noise measurements using a three-axis array of 28 low-frequency sensors. By recording the signals from the individual sensors it is possible to study the correlation as a function of sensor separation. Simultaneous measurements were made of the three components of the wind velocity.

In order to minimize the dependence upon wind speed, it is convenient to express the sensor separation in wave numbers. For this purpose the wind velocity is decomposed into a mean component (the convection velocity) and a fluctuating component. The time-varying signal in a stationary anemometer or microphone is assumed to result from a spatially varying field that is frozen in time moving across the anemometer at a velocity equal to the convection velocity (the Taylor hypothesis). The cyclic frequency ($F$) of the time-varying signals from a stationary sensor is related to the component of the wave number ($k_1$) in the direction of the convection velocity of the spatially varying field by the equation

$$F = k_1 v/2\pi, \tag{1}$$

where $v$ is the convection velocity.

## II. THE MEASURING SYSTEM

### A. The infrasound sensors

The infrasound sensors used in this study are of an original design and cover a frequency range of 0.1 to 200 Hz. They are made from piezoelectric bimorphs potted in polyurethane and housed in sections of PVC pipe. Figure 1(c) is a photograph of one of these sensors. Figures 1(a) and (b) picture the internal components. The housing [Fig. 1(c)] is made from a 2.5-in. section of 2-in. O.D. schedule 40 PVC pipe with end caps. Twenty-five 1.9-mm holes are bored in each end cap and four around the center of the cylindrical body. The pressure-sensing elements [Figs. 1(a) and (b)] consist of two pressure sensitive capsules made from four commercially available piezoelectric bimorphs. The bimorphs are 3.5 cm in diameter and have a resonant frequency of about 1.5 kHz. The capsules are constructed by cementing these bimorphs to each side of a brass ring. In order to compensate for temperature changes, one of the capsules has the piezoceramic surface turned to the outside of the capsule and the other has the ceramic turned to the inside. The two capsules are then wired in series. When wired in this way voltage changes produced by the thermal expansion and contraction of the bimorphs cancel and those produced by the bending of the bimorphs in response to pressure changes add. To further thermally insulate the sensors, the capsules are potted in polyurethane, wrapped in fiberglass, and enclosed in a PVC housing. In this configuration, the sensors had a negligible seismic response.

[a)]Portions of this work were presented in a paper entitled "The use of an infrasound microphone array to study wind noise spectra and correlation" at the 145th meeting of the Acoustical Society of America in Nashville, TN, 28 April–2 May 2003.

[b)]Electronic mail: dshields@mil-tec.com

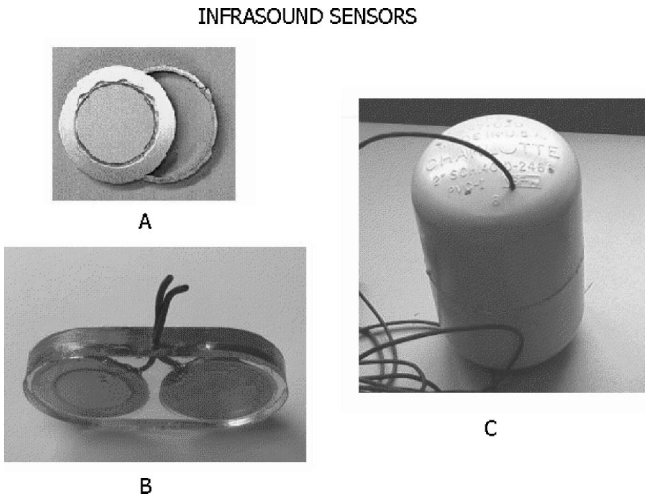


FIG. 1. Infrasound sensors. (a) pictures a piezoelectric "bimorph" formed by cementing a piezo-ceramic disc to a brass disc. A pressure sensitive capsule is formed by cementing one of these bimorphs to each side of the brass ring also shown. (b) pictures two capsules, one with the piezo-ceramic turned out and one with it turned in, potted in transparent polyurethane. (c) pictures the housing for the potted capsules. It is made from 2-in. schedule 40 PVC pipe with end caps. The potted capsules are wrapped in fiberglass and enclosed in this PVC housing. Fifty-four holes are bored in the PVC housing as explained in the text.

These sensors are high impedance, charge-generating devices and, as explained below, their sensitivity will depend upon the input impedance of the circuit used to measure their response. For the measurements reported here, the absolute sensitivity was not as important as the variation from sensor to sensor. The absolute sensitivity of the sensors was checked using a number of different techniques. For frequencies from 0.1 to 1 Hz, they were moved up and down in the atmosphere, being careful to avoid effects of acceleration and flow velocity of the air by the sensor. This method checked the response between 0.1 and 1 Hz (vertical displacement of 1 m in the atmosphere under standard conditions produces a change in pressure of 11.8 Pa). For frequencies between 0.1 and 10 Hz, they were placed in an airtight chamber fitted with a moveable piston. The pressure variation was determined by assuming that the volume changes produced by the piston motion were isothermal. For frequencies from 10 up to 100 Hz the response was compared to that of a model 4190 $\frac{1}{2}$-in. B & K microphone in sealed chambers of two different sizes. From these measurements, the absolute sensitivity using the detecting circuit described below was determined to be within 2 dB of 2 mv/Pa for frequencies between 0.1 and 100 Hz.

As for the variation from sensor to sensor, the individual sensors were compared to a reference sensor in a closed chamber. Only two of the sensors varied from the average by more than 12%. Each of the sensors was multiplied by a calibration constant so that all of the sensors had the same sensitivity to within $\pm 3\%$ between 0.1 and 10 Hz. Their phase response over this frequency interval was uniform to $\pm 0.1$ rad.

Twenty-eight of these sensors have been arranged into a three-axis orthogonal array. Counting the one shared sensor, each arm contains ten sensors. The sensors were 0.61 m (2 ft) apart. The individual sensors in each arm were taped to pipes 3.2 cm in diameter. A Campbell Instrument Company CSAT 3 ultrasonic anemometer was mounted 3 m off the ground about 0.5 m from one of the pressure sensors on the vertical arm of the array.

Three analog outputs of the anemometer gave voltages that were proportional to the $x$, $y$, and $z$ components of the wind velocity. These voltages were output (updated) 60 times a second and were read with the same data acquisition card as the sensor voltages. By using the analog output of the anemometer the velocity measurements were synchronized with the pressure measurements with a 0.033-s delay.

### B. The data acquisition system

The sensor capsules described above are charge-generating devices with a capacitance of approximately 130 nF. As such, they require a high-input impedance detecting circuit. The voltages from the array were measured by connecting the sensors to the input of a National Instrument Company 6031E data acquisition card. This card has 64 single-ended or 32 differential input channels with an input impedance of 100 G$\Omega$ in parallel with a 100-pF capacitance. Its maximum sampling rate is 100 000 Hz. In order to avoid cross talk between successively read channels with this card when the sources have high internal impedance, it is necessary to read a shorted input between each two channel readings. This effectively increases the input capacitance of the digitizer by the sampling frequency. The metalized ceramic surfaces of the two capsules in the temperature-compensated transducers were wired to the differential inputs of the data acquisition board with the brass backing plates grounded. A 20-m$\Omega$ input shunting resistance was connected from each of the differential inputs to ground to limit the response for frequencies below 0.05 Hz where temperature fluctuations become a problem. The analog channels are scanned 500 times per second. For a single data file, voltage measurements from all of the channels were accumulated in a computer for 120 s. With this digitizer and sampling rate the sensors had a sensitivity of 2.0 mV/Pa between 0.05 and 10 Hz.

## III. THE SITES FOR THE MEASUREMENTS

The measurements reported here were made at three different sites. For each of them there were several hundred meters of unobstructed terrain in the direction of the prevailing wind. Figure 2 shows a photograph of the array deployed at site one, a sod field located about 8 miles south of Oxford, MS. The second site was a disked field (the soil surface broken up with clods a few inches in linear dimensions), and the third was a cotton field. The cotton had been picked, but the cotton stalks remained with a uniform height of about 70 cm. The prevailing wind was blowing across the cotton rows. In the data displayed in the figures below, six 2-min runs in the cotton field and the disked field and 15 2-min runs in the sod field have been averaged. The 15 runs in the sod field were taken on two different days under different weather

FIG. 2. The infrasound array as deployed in the sod field which was one of the sites for the measurements.

conditions. The convection velocities as measured 3 m above the ground varied between 4 and 8 m/s, with most of the measurements falling between 5 and 7 m/s.

## IV. THE AVERAGE RESPONSE FROM EACH ARM OF THE ARRAY

The power spectral density of the pressure variations for each of the three arms of the array for each of the three sites is plotted in Fig. 3. For this purpose, the 2-min data files for each run were Fourier analyzed using the MATLAB ''Spectrum'' program. The fast Fourier transform (FFT) calculation used 10 000 points (at the sampling rate of 500 Hz this corresponds to 20 s), an overlap of 5000 points, and a Hanning window. The spectra have not been normalized by dividing by 1/2 the sampling rate. Therefore, the area under the curves represents the variance of the pressure signals. The data for these curves were obtained from ten sensors in each arm of the array. The top curve, A, in each figure is obtained by calculating the spectra of time signals from each of the ten sensors in the arm and then averaging these spectra for all the runs at a given site. Therefore, the A curves represent the average spectrum from a single sensor in each arm. The average is for 60 spectrum curves for the disked and cotton fields and 150 for the sod field. For the lower curves (B), the time signals from the nine sensors of each arm of the array were instantaneously summed and divided by the number of sensors to obtain an average time signal. The spectra of these average time signals were calculated for each run and then these 6 or 15 spectra averaged for each site. For these B curves then, if the sensors are far enough apart so that their signals are uncorrelated, this averaging of the time signals should divide the noise power density by the number of sensors. This is seen to be the case for the vertical arm signals at all three sites for frequencies above approximately 1 Hz. For the two horizontal arms that are on the ground the wind noise at the higher wave numbers is reduced to where the spectra are influenced by background sound. Since the sound is at

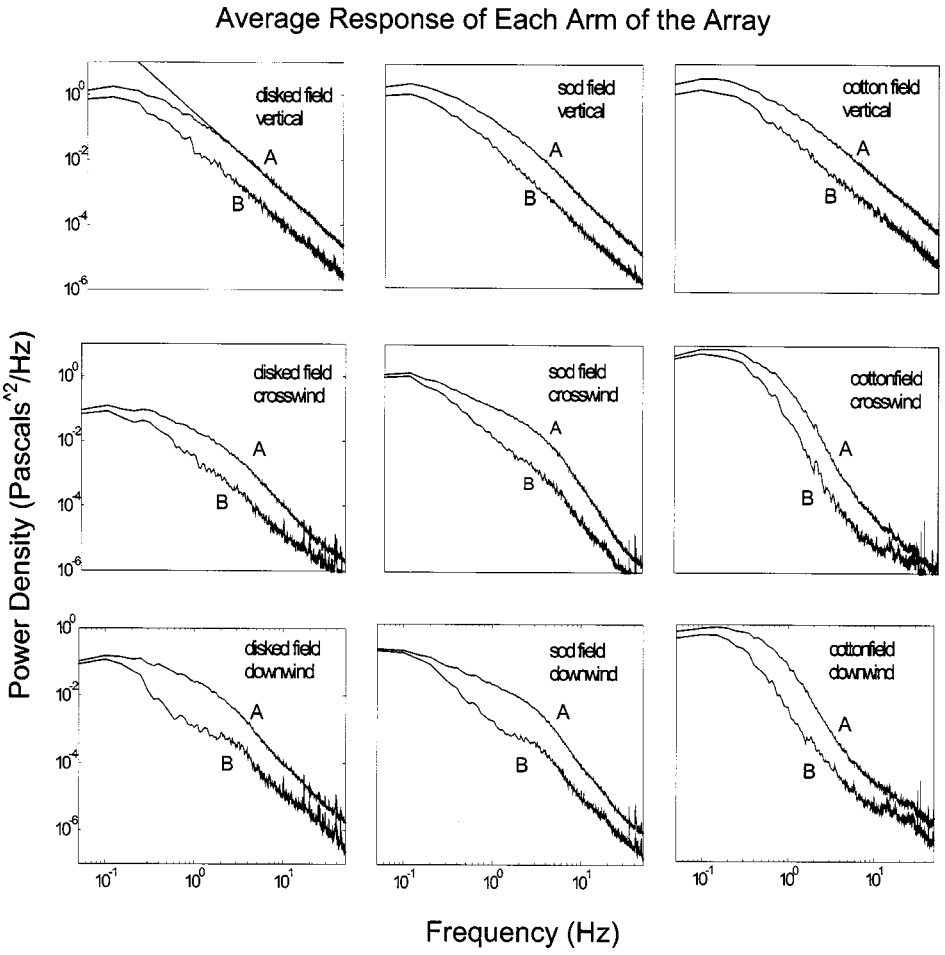


FIG. 3. The power spectral density of the varying pressure as measured by each arm of the array at each of the three sites. Curves A were obtained by averaging the spectra from ten sensors in each arm. Curves B were obtained by taking the spectra of the average signal from the same ten sensors.

least partially correlated over the arm of the array, averaging the time signals reduces the power level by less than the $1/n$ factor.

The average spectrum for the ten sensors in the vertical arm that are from 0 to 18 ft off the ground has very nearly a $-\frac{7}{3}$ slope. This is illustrated by the straight line plotted through the data for the vertical arm in the disked field. For the horizontal arms on the ground, the surface boundary reduces the turbulence and causes a deviation of the spectral slopes from $-\frac{7}{3}$. The spectra for the cotton field data differ significantly from the other two sites. The noise level in the vertical arm is greater and the shape of the spectra for the two arms on the ground is different. The pressure levels at frequencies in the neighborhood of 0.3 Hz are increased while those around 3 Hz are decreased. Other unique aspects of the cotton field data are discussed below.

For the disked field and sod field, averaging the signals from the downwind arm produces greater than $1/n$ noise reduction for wave frequencies between about 0.5 and 5 Hz. This can be explained by assuming that the turbulent pressure field has a periodicity. When the convection velocity carries this periodic field across the downwind arm of the array, for wavelengths comparable to the length of the array arm, signals from different parts of the array will be out of phase and cancel out in the averaging process. This effect is examined more carefully in the next section.

## V. CORRELATION STUDIES

It is interesting to compare the measurements made here with those made by J. T. Priestley nearly 40 years ago. He made narrow-band pressure correlation measurements in the frequency range 0.008 to 1 Hz for wind speeds ranging from 2.1 to 7.2 m/s. He used six pressure sensors constructed at the Bureau of Standards to study the dependence of the correlation on the downwind and crosswind separation of the sensors.[4] He determined, in agreement with earlier studies, that the narrow-band correlation coefficients in the down wind and crosswind directions are given by

$$R(\text{downwind}) = e^{-\alpha x}\cos(k_1 x) \tag{2}$$

and

$$R(\text{crosswind}) = e^{-\beta y}, \tag{3}$$

with $x$ and $y$ the downwind and crosswind separations. Priestley found that, though the convection velocity given by $(2\pi^* F/k_1)$ was highly dependent upon meteorological variables, the functional relationships between $\alpha$, $\beta$, and $k_1$ were remarkably independent of them. ($F$ was the center frequency of his filtered signal and $k_1$ chosen to fit his data.) He obtained[5]

$$\alpha = 0.33 \cdot k_1^{1.28} \quad \text{for } 0.5 < 1/k_1 < 50, \tag{4}$$

$$1/\beta = 0.84 \cdot (1/\alpha)^{0.74} \quad \text{for } 3 < (1/\alpha) < 500, \tag{5}$$

where $\alpha$ and $\beta$, are measured in reciprocal meters and $k_1$ in radians per meter.

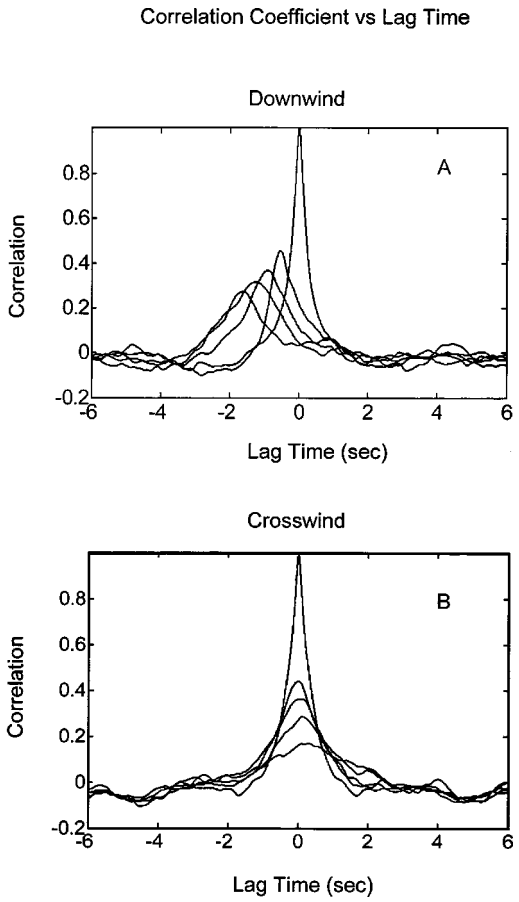


FIG. 4. The correlation coefficient versus the lag time for signals from five sensors in (a) the downwind arm of the array and (b) the crosswind arm of the array. For the crosswind arm the sensors are separated by 2 ft (61 cm) and for the downwind arm they are separated by 4 ft (122 cm).

It should be noted in comparing these constants to those reported here for measurements at larger wave numbers, a value of $\alpha$ proportional to $k_1$ to the first power fits his data for wave numbers between 0.5 and 2 $\text{m}^{-1}$.

To study the correlation in the data taken here, signals from each arm of the array have been analyzed using the MATLAB XCOV program. This program calculates the cross correlation between the signals as a function of lag time. Figures 4(a) and (b) shows this correlation for signals from five sensors in the downwind and crosswind arms of the array, respectively, for the disked field data. Plotting the correlation at zero lag time versus sensor separation in these two figures gives the decrease in correlation with distance in the crosswind and downwind directions. Plotting the peak heights versus lag time for the downwind arm [Fig. 4(a)] gives the decrease in correlation with time at a fixed position in the turbulent pressure pattern (according to the Taylor hypothesis). As has been pointed out by Bass, Raspet, and Messer, the convection velocity should equal to the slope of the plot of the sensor separation versus lag time at which the peak of the curves in Fig. 4(a) occurs.[6]

It is interesting to look at these correlation curves as a function of frequency. For this purpose the digitized time domain signals are filtered with a fourth-order bandpass Butterworth filter with the high- and low-pass frequencies the same. Figures 5(a)–(c) show the correlation of the signals at

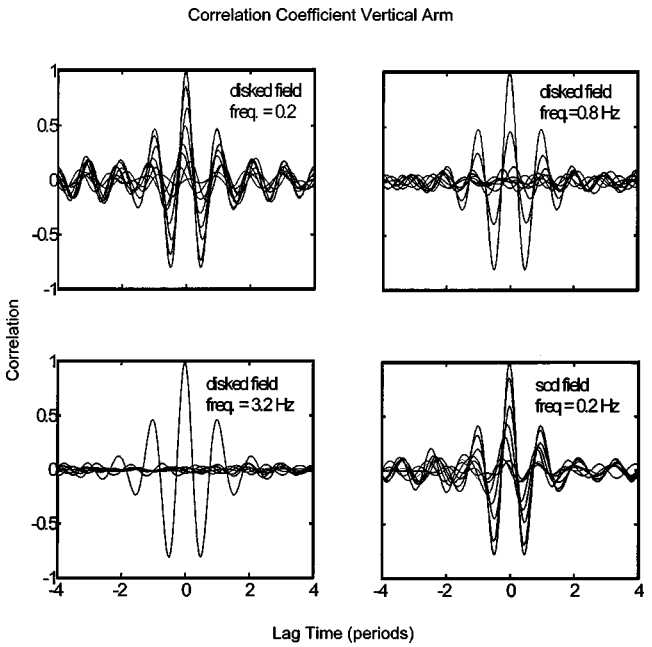


FIG. 5. Single-frequency correlation versus lag time in periods for varying pressure signals from eight sensors in the vertical arm of the array.

three different frequencies from eight sensors in the vertical arm of the array for the disked field data. The sinc function shape of the correlation curves is characteristic of the correlation of a narrow band of frequencies. The lag time has been normalized by dividing by the period of the filtered signal. This gives the same shape to curves at different frequencies. As the frequency is increased from 0.2 Hz in Fig. 5(a) to 3.2 Hz in Fig. 5(c), the rate of decrease in correlation with distance rapidly increases to where at 3.2 Hz there is negligible correlation even between the adjacent sensors that are separated by only 0.6 m. Figure 5(d) gives the curves for the same frequency as Fig. 5(a) but for the sod field. The correlation for the two sites is very similar.

Figure 6 is a plot of the correlation at zero lag time between sensors in the downwind arm of the array versus the sensor separation in wavelengths. Data for the disked, sod, and cotton fields for a number of frequencies have been plotted on the same graph. The data for each site have been

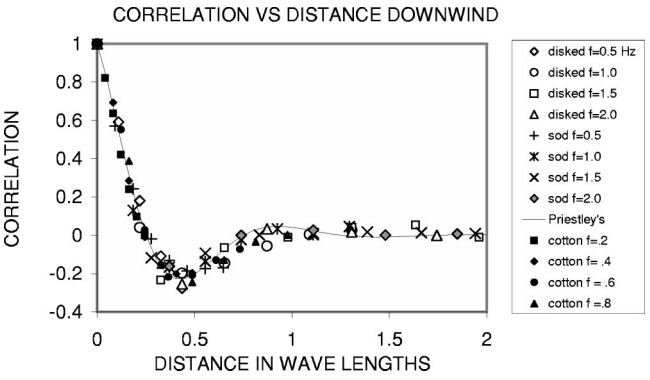


FIG. 6. Correlation of the varying pressure signals versus the sensor separation in wavelengths in the downwind direction. The data are for four different frequencies and for three different sites as designated in the legend. The solid curve is the fit to Priestley's data taken at much lower frequencies in 1964.

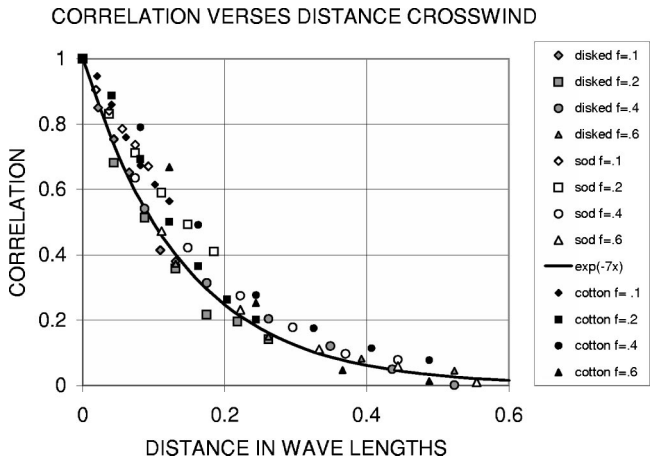


FIG. 7. Correlation of the varying pressure signals versus the sensor separation in wavelengths in the crosswind direction. The data are for four different frequencies and for three different sites as designated in the legend. The solid exponential curve is drawn visually to fit the data.

averaged not only for all runs at the site, but also for all pairs of sensors with the same separation. The wavelength was determined by dividing the convection velocity by the frequency of the filter. However, since the sensors are on the ground, the anemometer measurement of the velocity made 3 m above the ground is inadequate because of near-surface wind shear. Instead the convection velocity for the three sites was adjusted to make the data fit Eq. (2). These velocities were 2.8, 3.3, and 3.0 m/s for the disked, sod, and cotton fields, respectively. The velocities obtained in this way were approximately equal to those obtained from the plot of the sensor separation versus the lag times at which the maximum in the correlation occurs (see Fig. 4). The average velocities for the three sites measured with the anemometer 3 m above the ground were 6.2, 6.7, and 5.9 m/s, respectively.

To within experimental error, the correlation is seen to be a function of the separation divided by the wavelength independent of frequency, wind velocity (over the limited range of velocities measured), and even the terrain. Priestley references a number of authors who observed this functional relationship back in the 1960s.[4] The customary plot is correlation verses $2\pi$ times the abscissa in Fig. 6.

It is interesting to compare Priestley's measurements made many years ago in a grassy field near Dulles International Airport, Washington, DC, at much lower frequencies than those reported here. His $\alpha$ as given by Eq. (2) is slightly frequency dependent. The $\alpha$ value used to draw the curve in Fig. 6 corresponds to Priestley's $\alpha$ as calculated from Eq. (4) with a wave number of 4.7 $m^{-1}$. This is the highest wave number for the data plotted in Fig. 6.

Also of interest is the variation in the correlation coefficient with sensor separation in the crosswind and vertical directions. Figures 7 and 8 plot this dependence for the same runs and same convection velocities as Fig. 6. For Fig. 8 the separation is in the vertical direction between sensors that are 1.2 to 5.5 m above the ground. To within the accuracy of the measurements, the decay can be plotted as a function of the separation in wavelengths independent of frequency for the disked field, but for the sod and cotton fields the low frequencies decay slower in the crosswind direction and faster

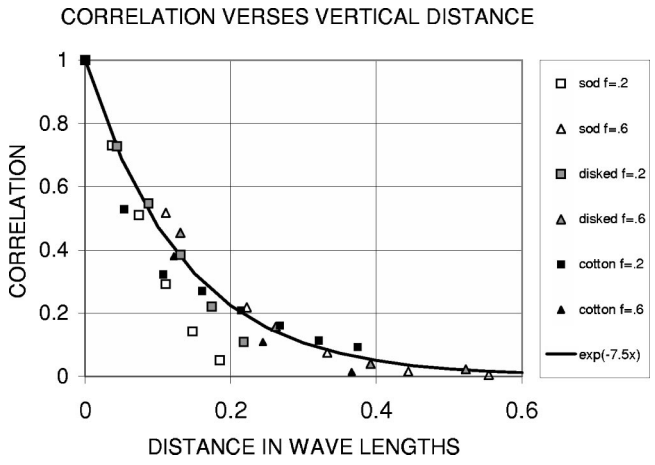


FIG. 8. Correlation of the varying pressure signals versus the sensor separation in wavelengths in the vertical direction. The data are for two different frequencies and for three different sites as designated in the legend.

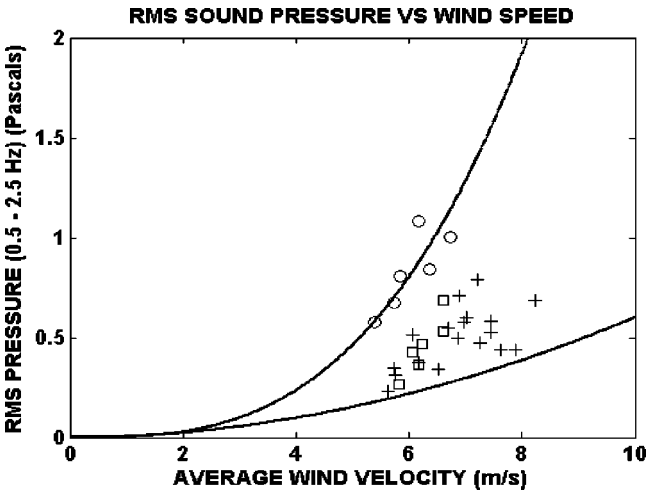


FIG. 9. The root mean square pressure variations in the frequency interval between 0.5 and 2.5 Hz plotted versus the average wind speed. Data are shown for six runs in the cotton field, six runs in the disked field, and 18 runs in the sod field. Circles are for the cotton field, squares are for the disked field, and crosses are for the sod field.

in the vertical direction. An exponential curve has been drawn visually through the data in Figs. 7 and 8 with a decay constant of approximately $-7$ per wavelength for the crosswind and $-7.5$ for the vertical direction. Priestley measured the crosswind decay and got a decay constant that was slightly frequency dependent. For the frequency range reported his value would be about 3.5, or about half of our measurement.

## VI. VELOCITY AND PRESSURE SPECTRA

### A. Validation of the pressure measurements

Widely different results are reported for pressure spectrum measurements in turbulence.[7–13] One must always be concerned with what is being measured by a pressure sensor in turbulent flow.

Of first concern is the disturbance introduced by the sensing element. Even when this is minimized, Morgan and Raspet conclude, ''The dominant source of wind noise in outdoor microphones is the pressure fluctuations caused by the velocity fluctuations of the incoming flow.'' [13] To study this question further, sensors employed here were oriented in different directions relative to the wind direction and the spectra of their response compared. This response was found be insensitive to orientation relative to wind direction over the frequency range of interest. In addition, their response in wind has been compared to the response obtained using a ''Quad Disk.'' [14] This device is designed to measure pressure independent of wind direction and magnitude. Bedard *et al.* have used it to measure pressure variations in a 0.5- to 2.5-Hz band over a 3-month period.[15] Their results differ significantly from one period of measurement to another. They plot rms pressure variations in Pascals versus wind speed in meters per second. Their data for two different sample periods are fit with two equations, $dp = 0.0036\ U^{3.02}$ and $dp = 0.0063\ U^{1.98}$, where the pressure is in Pascals and the velocity in meters per second. [Bedard's Eq. (15) for his Dec. 11 data evidently has a factor of 2 missing.] Figure 9 shows a similar plot of measurements made here with the single sensor close to the anemometer in the vertical arm of the array averaged over the same frequency interval. The solid curves are plots of the two functions that fit Bedard's two sets of data.

As a further comparison of the response of our sensors with that of the Quad Disk, a B&K $\frac{1}{2}$-in. microphone was sealed in the axial tube of the Quad Disk and the Quad Disk and one of our sensors placed at a height of 3 m in the wind at the local airport. The power density spectra of the two devices are shown to agree remarkably well in Fig. 10. In this figure, 25 min of data were analyzed as explained in the discussion of Fig. 3. The average wind velocity was 4.6 m/s.

### B. The wavenumber dependence of the pressure and velocity spectra

Spectra of turbulence are generally explained by assuming that energy is fed into the turbulence at small wave numbers and is dissipated by viscous losses at high wave num-

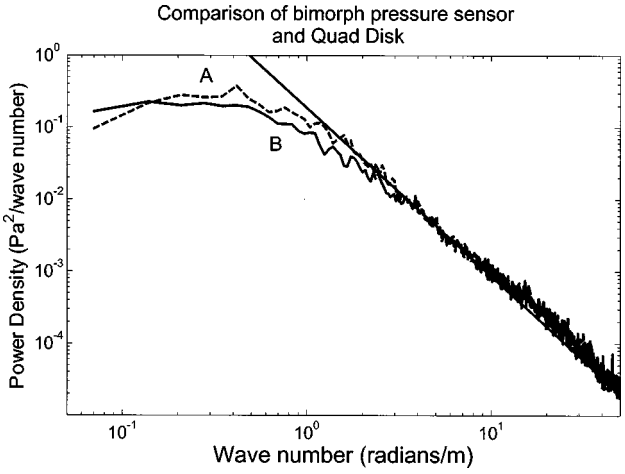


FIG. 10. The comparison of the power spectral density of 25 min of wind noise data taken with (a) the quad disk (dashed line) and (b) one of the sensors used to take the data reported here (solid line). Both were approximately 3 m off the ground and approximately 5 m apart. The straight line through the data has a slope of $-\frac{7}{3}$. The wind speed was 4.7 m/s.

bers. The energy cascades from large eddies to smaller ones. For a homogeneous turbulent field there will be a range of wave numbers called the inertial subrange where there is negligible production and dissipation of turbulent energy. In this range of wave numbers the one-dimensional velocity spectrum from symmetry considerations is expected to obey the equation[16]

$$F_1(k_1) = a_v k_1^{-5/3}. \tag{6}$$

Here $F_1$ is the power spectral density of the component of the varying velocity in the direction of the convection velocity, and $a_v$ is independent of frequency but depends upon the rate of energy dissipation in the turbulent field. If the turbulence is isotropic over this range of wave numbers, the spectra for the other two velocity components in the $k_1$ direction have a similar form with $a_v$ multiplied by $\frac{4}{3}$ and have a negligible correlation with each other. The three conditions, $-\frac{5}{3}$ power law, $\frac{4}{3}$ ratio between the transverse and longitudinal velocity components, and the vanishing (or very low) co spectral levels, are used as a test for the existence of an inertial subrange.[16]

From dimensional analysis the power density of the dynamic pressure (i.e., $p/\rho$) in the inertial subrange is expected to vary as[17]

$$F(P/\rho) = a_p k_1^{-7/3}, \tag{7}$$

with $a_p$ independent of frequency but dependent upon the rate of energy dissipation in the turbulent field. However, the exponent of the wave number is contested by both experiment and theory.[7,11]

The range of wave numbers over which the turbulent fields studied here might be considered homogeneous, and therefore the range over which the inertial subrange equations might be expected to apply, is limited on the high side by the dimension of the sensor and anemometer (approximately 0.1 m) and on the low side by the height the sensor and anemometer were above the ground (approximately 3 m). The spectra for the sensors on the ground would not be expected to demonstrate the inertial subrange frequency dependence. These conditions would limit the inertial subrange to wave numbers between approximately $2\pi/0.2$ and $2\pi/6$ m, or between 30 and 1 rad/m.

Figure 11 shows the averaged power spectral densities calculated using MATLAB software as explained in discussing Fig. 3 above. The A curves are for the variations in the kinematic pressure (i.e., pressure divided by the density of air). The B curves are for the variations in the component of the velocity in the direction of the convection velocity. The pressure variations were measured by the single sensor located about 0.5 m from the anemometer. Both were approximately 3 m off the ground. The spectra for each 2-min run were calculated in units of per radian of distance by specifying the sampling rate in samples per radian of distance which is equal to $2\pi$ times the samples per second divided by the convection (average) velocity for each run. These spectra (6 for the disked and cotton fields and 18 for the sod field) were averaged and plotted in Fig. 11. This plot of the component of the varying velocity in the direction of the convection velocity and the pressure divided by the air density against

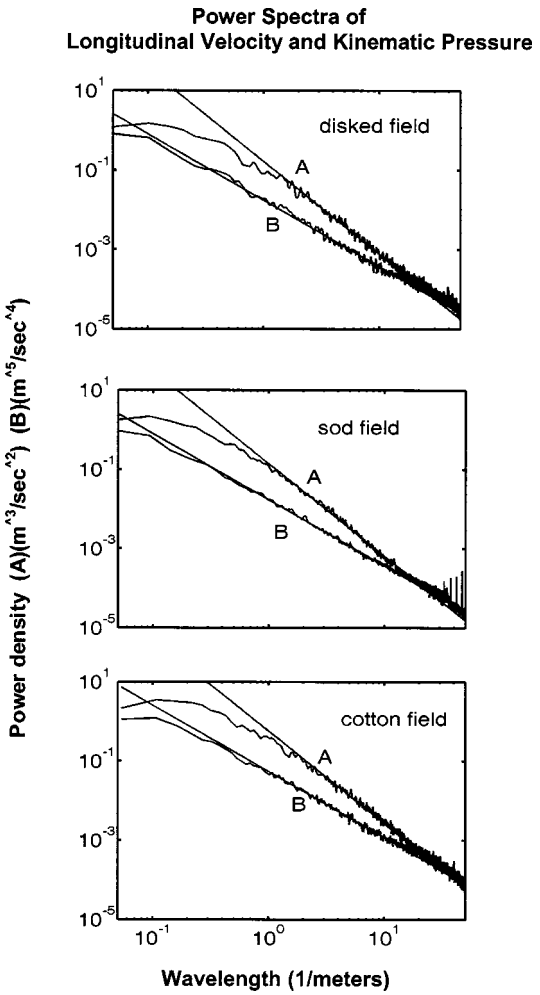


FIG. 11. The power density spectra for the varying wind velocity and pressure as measured at three different sites. Curves A are for velocity and curves B for pressure.

the wave number in the direction of the convection velocity was used because these are the quantities frequently calculated theoretically. The curves would be changed insignificantly if the spectrum of the total varying velocity were plotted.

The straight lines drawn through the curves have slopes of $-\frac{5}{3}$ for the velocities and $-\frac{7}{3}$ for the pressures. The constant multiplying factors are adjusted to give the best fit between 1 and 10 $m^{-1}$.

As a further test for the inertial subrange, similar curves were plotted for the transverse components of velocity. As stated above, if the turbulent field is isotropic, the ratio of the power density of the transverse to the longitudinal components should equal $\frac{4}{3}$. For the average of 36 min of sod field data and 12 min of the disked field data, this ratio is approximately equal to $\frac{4}{3}$. However, for the average of 12 min of cotton field data this ratio is approximately 1. These are the same data used in the correlation studies. For all three sites the ratio of the power density of the vertical component to the downwind component is approximately 1. The third condition for the inertial subrange, i.e., small or vanishing cospectra between the different velocity components, is met by the $x$ and $y$ velocity components in the sod and disked fields, but the $x$ and $y$ components in the cotton field and the $x$ and

$z$ components at all three cites showed a maximum correlation of approximately 0.2.

## VII. CONCLUSIONS

(1) The noise power reduction produced by averaging signals from nine individual sensors varied as 1/(number of sensors) for a range of frequencies when the sensor spacing was greater than a few tenths of the wavelength in the turbulent pressure field, where the wavelength is determined by dividing the convection wind velocity by the frequency.
(2) The frequency-dependent correlation of the wind noise over a range of wind velocities and atmospheric and environmental conditions varies as $\exp(-3.2x)\cos(2\pi x)$, where $x$ is the sensor separation in wavelengths in the down wind direction. This allows greater than $1/n$ noise reduction if the aperture of the array is greater than $\frac{1}{4}$ wavelength of the pressure variations in the wind.
(3) The correlation as a function of sensor separation for arrays in the crosswind and vertical directions is given approximately by $\exp(-7x)$ for a range of wind velocities and atmospheric and environmental conditions.
(4) For frequencies expected to fall within the inertial subrange, the $-\frac{5}{3}$ law for the velocity spectrum and the $-\frac{7}{3}$ law for the pressure spectrum were found to hold.

## ACKNOWLEDGMENTS

The help of Chris Clark and Brandon Smith in taking data is gratefully acknowledged. Thanks also go to Dr. Ken Gilbert, Dr. Carrick Talmadge, Dr. Richard Raspet, Dr. Garth Frazier, and Dr. Henry Bass for helpful discussions, and to the U.S. Army Armament Research Development and Engineering Center for supporting this work.

[1] F. B. Daniels, "Noise-reducing line microphone for frequencies below 1 cps," J. Acoust. Soc. Am. **31**, 529–531 (1959).
[2] S. M. Tenney, B. T. Mays, and J. M. Noble, "A methodology for infrasonic detection and array signal processing," Army Research Laboratory, Security Office, 2800 Powder Mill RD. Adelphi, MD 20783 (1999).
[3] M. A. Hedlin, B. Alcoverro, and G. D'Spain, "Evaluation of rosette infrasonic noise reducing spatial filters," J. Acoust. Soc. Am. **114**, 1807–1820 (2003).
[4] J. T. Priestley, "Correlation Studies of Pressure Fluctuations on the Ground Beneath a Turbulent Boundary Layer," National Bureau of Standards Report No. 8942 (1965); also M.S. thesis, University of Maryland (1965).
[5] J. T. Priestley, "Calculation of the Effectiveness of Infrasonic Line Microphones for Reducing Wind Noise," National Bureau of Standards Report 9380 (1966). This report corrects a mistake in the value of alpha given in the 1965 report.
[6] H. E. Bass, R. Raspet, and J. O. Messer, "Experimental determination of wind speed and direction using a three microphone array," J. Acoust. Soc. Am. **97**, 695–696 (1995).
[7] W. K. George, P. D. Beuther, and R. E. A. Arndt, "Pressure spectra in turbulent free shear flows," J. Fluid Mech. **148**, 155–191 (1948).
[8] J. M. Wilczak, S. P. Oncley, and A. J. Bedard, Jr., "Turbulent pressure fluctuations in the atmospheric surface layer," *Proc. 10th Symposium on turbulence and diffusion*, Portland, OR (Am. Meteor. Soc., Boston, MA, 1992, pp. 167–170).
[9] J. D. Albertson, G. G. Katul, M. B. Parlange, and W. E. Eichinger, "Spectral scaling of static pressure fluctuations in the atmospheric surface layer: the interaction between large and small scales," Phys. Fluids **10**, 1725–1732 (1998).
[10] Y. Tsuji and T. Ishihara, "Similarity scaling of pressure fluctuation in turbulence," Phys. Rev. E **68**, 026309 (2003).
[11] A. I. Grachev and M. I. Mordukhovich, "Spectrum of pressure fluctuations in the atmospheric ground layer," Izv., Acad. Sci., USSR, Atmos. Oceanic Phys. **24**, 159–160 (1988).
[12] H. V. Fuchs, "Measurement of pressure fluctuations within subsonic turbulent jets," J. Sound Vib. **22**, 361–378 (1972).
[13] S. Morgan and R. Raspet, "Investigation of the mechanisms of low frequency wind noise generated outdoors," J. Acoust. Soc. Am. **92**, 1180–1183 (1992).
[14] R. T. Nishiyama and A. J. Bedard Jr., "Quaddisc static pressure probe for measurements in adverse atmospheres: With a comparative review of static pressure probe designs," Rev. Sci. Instrum. **62**, 2193–2204 (1991).
[15] A. J. Bedard, R. W. Whitaker, G. E. Greene, P. Mutschlecner, R. T. Nishiyama, and M. Davidson, "Measurements of pressure fluctuations near the surface of the earth," *Proc. 10th Symposium on turbulence and diffusion*, Portland, OR (Am. Meteor. Soc., Boston, MA, 1992, pp. 293–296).
[16] J. C. Kaimal and J. J. Finnigan, *Atmospheric Boundary Layer Flows* (Oxford U. P., Oxford, 1994), pp. 36 and 37.
[17] A. S. Monin and A. M. Yaglom, *Statistical Fluid Mechanics* (MIT, Cambridge, 1975), Vol. 2, p. 374.